A comprehensive survey of M_2AX phase elastic properties

2009 J. Phys.: Condens. Matter 21 305403

(http://iopscience.iop.org/0953-8984/21/30/305403)

J. Phys.: Condens. Matter **21** (2009) 305403 (9pp) doi:10.1088/0953-8984/21/30/305403

A comprehensive survey of M_2AX phase elastic properties

M F Cover, O Warschkow, M M M Bilek and D R McKenzie

School of Physics, The University of Sydney, New South Wales, 2006, Australia

E-mail: o.warschkow@physics.usyd.edu.au

Received 30 January 2009, in final form 20 May 2009
Published 8 July 2009
Online at stacks.iop.org/JPhysCM/21/305403

Abstract

M_2AX phases are a family of nanolaminate, ternary alloys that are composed of slabs of transition metal carbide or nitride (M_2X) separated by single atomic layers of a main group element. In this combination, they manifest many of the beneficial properties of both ceramic and metallic compounds, making them attractive for many technological applications. We report here the results of a large scale computational survey of the elastic properties of all 240 elemental combinations using first-principles density functional theory calculations. We found correlations revealing the governing role of the A element and its interaction with the M element on the c axis compressibility and shearability of the material. The role of the X element is relatively minor, with the strongest effect seen in the in-plane constants C_{11} and C_{12}. We identify several elemental compositions with extremal properties such as W_2SnC, which has by far the lowest value of C_{44}, suggesting potential applications as a high-temperature dry lubricant.

S Supplementary data are available from stacks.iop.org/JPhysCM/21/305403

1. Introduction

M_2AX phases [1, 2] are a class of materials composed of three elements (figure 1): an early transition metal (M), a main group element (A), and either carbon or nitrogen (X). M_2AX phases are characterized by a nanolaminate structure in which slabs of the carbide/nitride (M_2X) are separated by single atomic layers of the A element. This layered structure results in a unique combination of ceramic and metallic properties [3]. M_2AX phases mimic ceramics in that they are stiff [4], resistant to oxidation [5], and are believed to remain strong at temperatures exceeding 1400 °C [6]. The metal-like properties of M_2AX phases manifest themselves in their machinability [7], resistance to thermal shock [8], high damage tolerance [9], and electrical [10] and thermal conductivity [11]. This combination of metallic and ceramic properties is attractive for a number of technological applications, including use as a high-temperature structural material where M_2AX phases could greatly exceed the capabilities of current metal alloy materials.

Elastic properties are of particular interest as they determine important macroscopic properties such as lubrication, friction, and machinability. Experimental investigation of M_2AX phase elastic properties has been hindered by the difficulties associated with producing phase pure samples [12].

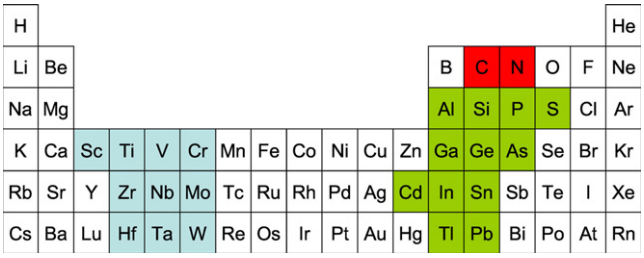

Figure 1. Periodic table of the elements in which those elements that participate in M_2AX phase formation are highlighted in shades of grey (colour). The M elements are shaded light grey (blue), the A elements medium grey (green) and the X elements dark grey (red). (This figure is in colour only in the electronic version)

This makes theoretical investigations important tools in understanding these materials as they can be used to analyse phases that have not been experimentally prepared. The large number of elemental combinations of the M_2AX phases suggests a wide tunability of materials properties which could be mapped out using theory. Several theoretical studies [13–19] have already considered the elastic properties of selected M_2AX phases. However, these studies have been limited to small subsets of the M_2AX phase family. Furthermore, calculated

Table 1. The generic crystal structure of a M_2AX phase (space group $P6_3/mmc$, #194). The independent variables particular to each elemental composition are the hexagonal lattice constants a and c, as well as z_M, the vertical position of the M element.

Element	Wyckoff	x/a	y/b	z/c
M	(4f)	1/3	2/3	z_M
A	(2d)	1/3	2/3	3/4
X	(2a)	0	0	0

constants often vary considerably between different groups due to differences in methodology, thus preventing effective comparisons. A single, comprehensive study covering all elemental combinations is required to provide global insights into the underlying structure/property relationships.

High throughput combinatorial surveys of material properties have a number of precedents in applications such as binary alloys [20–23], alloy surface catalysts [24–26], cathode materials for use in batteries [27], and fuel cell anode catalysts [28]. Common to these studies is a computational survey over a large number of elemental and structural combinations to identify property trends of interest. This generally requires a robust and well-defined computational method that can be applied universally to all combinations so that calculated properties can be compared. The method must also be efficient enough so that all combinations can be calculated. This may result in a choice of method that may not be ideal in terms of accuracy, yet good enough to screen a large number of combinations for interesting compositions. To this end, density functional theory offers a good balance between computational efficiency and predictive accuracy. Inspired by these principles, we formulate a procedure to calculate elastic constants and derived properties of all 240 elemental combinations of the M_2AX phase family. The resulting data base of elastic properties (provided in full as supplementary data available at stacks.iop.org/JPhysCM/21/305403) is data mined for structure/property correlations and trends. We identify several M_2AX phases that feature extremal elastic properties.

2. Methods

2.1. M_2AX phase structure

The generic crystallographic positions of a M_2AX phase are summarized in table 1. The structure is broadly characterized by a highly symmetric hexagonal unit cell containing atomic layers of M, A, and X elements stacked along the c direction. Each X layer of atoms is sandwiched between two M layers to form a slab of M_2X composition with a local fcc-type stacking sequence. Single atomic layers of the A elements separate these slabs. The local stacking around the A atomic layer follows a hcp style pattern so that the A layer forms a mirror plane in the crystal. Due to high symmetry, the crystal structure is fully defined by the a and c lattice vectors and the interplanar separation d_{MX} between M and X atomic layers. The interplanar separation d_{MX} is derived from the internal parameter z_M by $d_{MX} = cz_M$. The interplanar separation between M and A atomic layers d_{MA} is given by $d_{MA} = c(1/4 - z_M)$.

2.2. Density functional theory

All calculations in this work are carried out using density functional theory (DFT) and the planewave/core potential formalism implemented in the VASP software [29–31]. Core electrons are represented using projector-augmented wave (PAW) core potentials [32, 33]. The eigenfunctions of valence and near-valence electrons are expanded in terms of a planewave basis. Electron exchange and correlation are treated in the generalized gradient approximation using the PW91 functional [34].

To avoid the need to optimize computational parameters such as **k**-point density and planewave cutoff for all 240 M_2AX phases considered in this work, we choose three representative *trial phases*: Ti_2SiC, W_2AlC, and Cr_2SnN. We believe that these adequately cover the elemental diversity of the M, A, and X elements. Our parameter choices are validated against these three trial structures.

Integrations over the Brillouin zone of the M_2AX phase hexagonal unit cells are performed using discrete Γ-centred grids of 15 × 15 **k**-points in the reciprocal a, b-plane and 5 points along c. For our three trial phases, the calculated energy is converged to within 3 meV (per M_2AX formula unit) of the limiting value at large cutoff.

We use a universal planewave energy cutoff of 500 eV in our calculations. This is above the recommended cutoff for all the elemental core potentials used in our survey. For the three trial phases, the total energies calculated with this cutoff are converged to within 5 meV (per formula unit) of the highest cutoff tested (900 eV). Further tests confirmed that an increase of the cutoff from 500 to 700 eV would result in changes in the calculated elastic constants C_{ij} of less than 1 GPa. Our choice of a 500 eV cutoff is also in line with previous PAW–DFT studies on M_2AX phases [13, 14, 35–37]. The planewave cutoff for the augmentation charge density is set to 1500 eV.

In our geometry optimizations, we use a force component convergence criterion of 0.01 eV $Å^{-1}$ which we confirmed through testing to be adequate for the purpose of this work.

2.3. Calculation of elastic constants

The elastic constants C_{ij} relate the stress σ_i of a material to the applied strain α_j. These constants can be conveniently calculated in one of two ways. In the *energy method* the unit cell is subjected to a number of finite size strains along several strain directions. The calculated energies E_{strain} are fitted to the quadratic equation

$$E_{strain} = E(0) + V_0 \sum_{i,j} \tfrac{1}{2} C_{ij} \alpha_i \xi_i \alpha_j \xi_j \qquad (1)$$

which is a simple Taylor expansion of E_{strain} in α to the second order. In this equation, we use the Voigt notation for the stress and strain directions, $E(0)$ is the energy of the relaxed cell, and V_0 is the relaxed volume of the cell. The factor ξ_j equals one for $j = 1, 2,$ or 3. For $j = 4, 5,$ and 6, ξ_j equals two [38]. In equation (1), there is no term that is linear in α, because the expansion is centred about the relaxed cell.

Table 2. The energy and stress equations as a function of the strain magnitude α for the five strain directions given by Fast *et al* [38].

Strain	Energy method	Stress method
1	$E(\alpha) = E(0) + V_0(C_{11} + C_{12})\alpha^2$	$\sigma_1(\alpha) + \sigma_2(\alpha) = 2(C_{11} + C_{12})\alpha$
2	$E(\alpha) = E(0) + V_0(C_{11} - C_{12})\alpha^2$	$\sigma_1(\alpha) - \sigma_2(\alpha) = 2(C_{11} - C_{12})\alpha$
3	$E(\alpha) = E(0) + \frac{1}{2}V_0C_{33}\alpha^2$	$\sigma_3(\alpha) = C_{33}\alpha$
4	$E(\alpha) = E(0) + 2V_0C_{44}\alpha^2$	$\sigma_5(\alpha) = 2C_{44}\alpha$
5	$E(\alpha) = E(0) + \frac{1}{2}V_0(2C_{11} + 2C_{12} + 4C_{13} + C_{33})\alpha^2$	$\sigma_1(\alpha) + \sigma_2(\alpha) + \sigma_3(\alpha) = (2C_{11} + 2C_{12} + 4C_{13} + C_{33})\alpha$

In the alternative *strain method* the stress–strain relation is used directly. Calculated stresses of the strained cells are fitted to the following linear equation:

$$\sigma_i = \sum_j C_{ij}\alpha_j\xi_j. \tag{2}$$

In both methods the strain is assumed small enough so that relaxations along the other strain directions can be neglected.

M_2AX phases, as hexagonal materials, are characterized by five unique elastic constants, namely C_{11}, C_{12}, C_{13}, C_{33}, and C_{44}. These constants are economically calculated using the five strains proposed by Fast *et al* [38] which result in a minimal loss of symmetry. Using this particular set of five strains, equations (1) and (2) are simplified to the forms given in table 2.

The VASP software calculates both the DFT energy and the stresses for a strained unit cell, thus we can use either the energy or the stress method to calculate elastic constants. After evaluating both methods, we decided to use the stress method in this work. The advantage of the stress method is that fewer strains are required for each direction to accurately fit the linear equations (see table 2). For each direction, we use two finite strains of magnitudes $\pm\alpha$ about the unstrained cell, leading to a three point fit to the linear stress equations. In contrast, the energy method used by Fast *et al* [38] uses four finite strains for a five point fit to the quadratic energy equations.

Both methods rely strongly on the assumption that the strain magnitudes α are small enough to ensure a linear stress–strain relation. However as α gets smaller, numerical errors become larger. Having tested values between ±0.001 and ±0.02, we chose a value of $\alpha = \pm0.01$ for the stress method because it gave the best agreement with the five point energy method for the three trial phases. Fast *et al* [38] recommend 0.01 and 0.02 for the energy method, so our choice of 0.01 for the stress method is consistent with their work.

After a strain is applied to our computational unit cell, we reoptimize the internal atomic positions because the cell distortion dislocates the atoms from their minimum energy positions. These internal reoptimizations are important as they significantly affect the calculated elastic constants. In addition, we found that internal reoptimization caused the energy and stress methods to produce more consistent results. We presume this occurs because the truncated expansions that underpin the stress and energy methods are affected differently by any residual internal stresses.

From the fitted elastic constants C_{ij} we compute several derived elastic properties including the elastic moduli (B, G, and E) and two types of performance parameter (μ_M and μ_D).

The bulk modulus (B) is a measure of the volume compressibility of a material and is given by:

$$B = \tfrac{2}{9}(C_{11} + C_{12} + 2C_{13} + C_{33}/2).$$

The shear modulus (G) quantifies the average shearability of a material. Following previous work [14], we use the Voigt approximation [39] to calculate the shear modulus as

$$G = \tfrac{1}{15}(2C_{11} + C_{33} - C_{12} - 2C_{13}) + \tfrac{1}{5}(2C_{44} + \tfrac{1}{2}(C_{11} - C_{12})).$$

We note that for the M_2AX phases, the most interesting shear plane is the [0001]-plane between the M_2X slabs and the A atomic layer. The relevant constant for this shear is C_{44}.

The Young's modulus (E) measures the response to a uniaxial stress averaged over all directions. It is obtained from the bulk and shear moduli using the expression for an isotropic material.

$$E = \frac{9BG}{3B + G}. \tag{3}$$

Two types of derived performance indicators are the ductility index, μ_D, due to Pugh [40], given by

$$\mu_D = B/G \tag{4}$$

and the machinability index, μ_M, due to Sun *et al* [41] which is defined as

$$\mu_M = B/C_{44}. \tag{5}$$

The underlying assumption of these two indices is that high tensile strength combined with low shear resistance leads to good machinability. The two indices give measures of this ratio, with one using C_{44} as the measure of shear resistance whilst the other uses G.

2.4. Computation procedure

Our large scale computational survey raises a number of technical issues that are worth noting. These are (1) loss of hexagonal symmetry during optimization, (2) multiple stationary points on a complex potential energy landscape, and (3) elastically unstable structures.

We optimized the geometry of a M_2AX phase crystal structure using a recursive, self-consistent protocol, in which the final structure of one optimization becomes the initial structure of the next. This is repeated until initial and final structures are the same. This ensures that the number of planewaves used to evaluate the final energy is consistent with the volume of the final structure and is not affected by the volume of the starting structure. The recursive process

Table 3. An example of a M_2AX phase with multiple stationary points on the potential energy surface. For each stationary point found, we report the energy per formula unit (in eV) and the lattice constants (in Å). Elastic constants (in GPa) are given for stable structures. For the unstable structure we report the Fast *et al* strain numbers (see table 2) that lead to structures of lower energy.

M_2AX	Energy	a	c	C_{11}	C_{12}	C_{13}	C_{33}	C_{44}
Mo_2SN	−34.757	3.340	10.96	301	196	145	267	19
	−34.501	3.019	12.55	308	180	218	381	130
	−34.370	3.169	11.73	unstable in 1, 2, 5				

occasionally results in the loss of hexagonal symmetry, which results in a much slower calculation as well as problems later on when strains are applied to the cell. To prevent this, we introduced a resymmetrization step between each cycle of the recursive reoptimization. This involved resetting the angles between the lattice vectors, equalizing the in-plane lattice vectors, and resetting the in-plane internal parameters to the high symmetry points.

In the course of our M_2AX phase survey we found that several of the compositions have more than one stationary point on the potential energy surface. These stationary points differ quite significantly in the lattice parameters a and c, as well as the calculated formation energy. For these phases the choice of starting structure determines the optimized structure. Details for one example, Mo_2SN, are given in table 3. For this phase we have identified three stationary points, two of which are stable in that they are minima on the potential energy surface. This is shown by the fact that the energy–strain equations (see table 2) have positive curvature in all five strain directions. The third stationary point found during optimization is not a minimum. Distortion of this structure along Fast *et al* strain directions 1, 2, and 5 resulted in structures of lower energy. We will assume here that the structure with the lowest energy is the global energy minimum. Relative to the global minimum, the other stable structure and the unstable structure are 0.26 eV and 0.39 eV higher in energy, respectively.

The finding of multiple minima for some phases raises questions. To what extent are our results for the other phases of our survey influenced by our choice of starting structure? How common is the multiple stationary point phenomenon in the M_2AX phase family? How sure can we be that we have found the global minimum for the phases that we consider? To these questions we cannot give a definitive answer, because the DFT optimization methods are generally *local* optimization methods. While there cannot be a guarantee that the global minimum has been found, multiple optimizations with differing initial structures dramatically increase the chances of finding it.

Phases with multiple stationary points appear to be limited to certain elements (mainly Mo and W) or element pairings (S–N). We established this by performing systematic optimizations with three different starting structures for phases that (1) were found to be elastically unstable, (2) exhibited a shallow minimum during the elastic constant calculation, or (3) are characterized by extremal properties. We believe this result affords a reasonable degree of confidence that most, if not all of the phases presented in our data are at their global minimum.

For 17 elemental compositions, we were unable to locate minimum energy structures with hexagonal M_2AX phase symmetry, despite multiple optimization attempts. These phases are:

V_2SN	Cr_2SN	Mo_2AlN	Mo_2SiN	Mo_2SC
Mo_2GeN	Mo_2InN	Mo_2SnN	W_2AlN	W_2SiN
W_2SC	W_2SN	W_2GaN	W_2GeN	W_2InN
W_2SnN	W_2PbC.			

In all these cases, a symmetry breaking strain (Fast *et al* strain 2 and/or 4, see table 2) leads to a non-hexagonal structure with lower energy. This suggests that the symmetric M_2AX phase structure is not the most energetically favourable structure for these combinations of elements, possibly explaining why these phases have not been observed experimentally.

3. Results and discussion

3.1. Error analysis

Our survey has given the structural and elastic properties of 240 M_2AX phases. The complete data set is provided as supplementary material, available from stacks.iop.org/JPhysCM/21/305403. We begin our analysis of this data with an estimate of the accuracy of these results. Sources of error include the intrinsic inaccuracy of the DFT formalism and the particular approach chosen to calculate elastic constants. We establish some measure of the magnitude of these errors by comparing our results with (1) experimental measurements, (2) theoretical elastic constants calculated by other groups, and (3) results obtained by a different method.

In table 4 we compare our elastic constants with experimental and theoretical constants reported in the literature. Looking first at the theoretical results, we see a considerable variation with many constants differing by up to 30 GPa between groups. The results from our work generally lie within the spread of results from other works. However the spread highlights the effect of the choice of computational method on the results. It is worth noting that we are using a more sophisticated approach than some (but not all) of the other works cited in that we relax the internal atomic positions in the strain calculations. Experimental results have only been obtained for the elastic moduli B, G, and E. Comparison of our results with experimental data shows a reasonable degree of agreement. In particular, comparison of our calculated moduli with the measurements reported by Hettinger *et al* [35] show agreement to within 10 GPa for the Nb_2AlC and Ti_2AlC phases; however for the V_2AlC and Cr_2AlC phases the moduli vary by up to 87 GPa. Differences in the experimental moduli reported by different groups indicate that there is considerable error in the experimental method as well.

In order to get a more detailed understanding of the effect of the method on specific elastic constants, we compare our constants, calculated with a three point stress method, with those obtained by a three point energy calculation. The three point energy calculation is certainly more approximate,

Table 4. Comparison of M_2AX phase elastic properties (in GPa) of this work with previous experimental and theoretical results in the literature. Results of this work are on the top line of each cell and are in bold.

M_2AX phase	Elastic constants (Theory)					B		G		E	
	C_{11}	C_{12}	C_{13}	C_{33}	C_{44}	Expt	Theory	Expt	Theory	Expt	Theory
V_2AlC	**339**	**71**	**100**	**319**	**148**		**171**		**134**		**319**
	338[a]	92[a]	148[a]	328[a]	155[a]	139[b]	215[b]	116[c]	128[a]	277[c]	308[a]
	346[d]	71[d]	106[d]	314[d]	151[d]	152[c]	175[d]		139[d]		306[d], 261[d]
							198[a]				
							197[e]				
Ti_2GaC	**303**	**66**	**63**	**263**	**101**		**139**		**109**		**260**
	314[f]	66[f]	59[f]	272[f]	122[f]		141[f]		121[f]		282[f]
V_2GaC	**334**	**81**	**111**	**299**	**138**		**175**		**125**		**302**
	343[f]	67[f]	124[f]	312[f]	157[f]		181[f]		133[f]		321[f]
Nb_2GaC	**309**	**80**	**138**	**262**	**126**		**177**		**108**		**270**
	374[f]	88[f]	135[f]	310[f]	149[f]		196[f]		132[f]		323[f]
Ta_2GaC	**335**	**106**	**137**	**315**	**137**		**194**		**118**		**294**
	420[f]	101[f]	146[f]	333[f]	175[f]		217[f]		151[f]		367[f]
Zr_2AlC	**261**	**63**	**63**	**224**	**87**		**125**		**92**		**221**
	278[g]	64[g]	67[g]	235[g]	97[g]		132[g]		100[g]		238[g]
Zr_2AlN	**264**	**77**	**89**	**235**	**105**		**141**		**94**		**231**
	285[g]	89[g]	92[g]	266[g]	129[g]		154[g]		107[g]		261[g]
Nb_2AlC	**310**	**90**	**118**	**289**	**139**		**173**		**116**		**285**
	341[d]	94[d]	117[d]	310[d]	150[d]	165[c]	183[d]	117[c]	131[d]	286[c]	288[d], 247[d]
	334[a]	115[a]	149[a]	324[a]	154[a]	128[b]	205[a]		119[a]		299[a]
Ta_2AlC	**334**	**114**	**130**	**322**	**148**		**193**		**122**		**303**
	354[a]	140[a]	159[a]	356[a]	172[a]		221[a]		126[a]		319[a]
Ti_2AlC	**302**	**62**	**58**	**270**	**109**		**137**		**114**		**267**
	321[a]	76[a]	100[a]	318[a]	144[a]	115[b]	171[b]	118[c]	128[a]	277[c]	305[a]
	307[g]	58[g]	63[g]	284[g]	118[g]	144[c]	141[g]		119[g]		279[g]
	308[d]	55[d]	60[d]	270[d]	111[d]		137[d]		118[d]		290[d], 250[d]
							166[e]				
							168[a]				
Ti_2AlN	**309**	**67**	**90**	**282**	**125**		**155**		**118**		**281**
	342[h]	56[h]	96[h]	283[h]	123[h]	107[b]	175[b]		122[h]		293[h]
	311[g]	71[g]	102[g]	298[g]	133[g]		163[g]		114[g]		276[g]
							163[h]				
Cr_2AlC	**365**	**84**	**102**	**369**	**140**		**186**		**138**		**332**
	396[a]	117[a]	156[a]	382[a]	173[a]	138[c]	203[b]	105[c]	147[a]	245[c]	358[a]
	384[d]	79[d]	107[d]	382[d]	147[d]	139[b]	193[d]		148[d]		347[d], 332[d]
							226[e]				
							226[a]				
Sc_2AlC	**175**	**59**	**33**	**191**	**44**		**88**		**57**		**140**
	186[i]	58[i]	40[i]	189[i]	48[i]		93[i]		60[i]		146[i]
Sc_2GaN	**214**	**60**	**57**	**214**	**70**		**110**		**75**		**183**
	177[i]	77[i]	44[i]	181[i]	45[i]		96[i]		53[i]		132[i]
Sc_2InC	**175**	**59**	**33**	**173**	**41**		**86**		**54**		**135**
	206[i]	51[i]	38[i]	191[i]	50[i]		95[i]		67[i]		160[i]
Sc_2TlC	**180**	**54**	**30**	**166**	**37**		**84**		**55**		**135**
	199[i]	52[i]	35[i]	172[i]	50[i]		90[i]		65[i]		154[i]

[a] See [14]; [b] see [36]; [c] see [35]; [d] see [15]; [e] see [37]; [f] see [18]; [g] see [17]; [h] see [13]; [i] see [19].

however it can be calculated without any additional overhead since the two strain calculations required have already been done. Table 5 lists for each of the elastic constants and moduli the mean, standard deviation and maximum value of the difference between the two methods. The table shows that some of the constants are more affected than others. C_{44} appears to be the least affected, with a mean difference of 1.8 GPa and 99.1% of the phases differing by less than 10 GPa. In contrast C_{13} appears to be the most affected, with a mean difference of 12.8 GPa and less than a third of the phases differing by less than 10 GPa. It is also instructive to look at the largest differences between the methods. Errors of more than 50 GPa occur in instances with C_{12} and C_{33}. The errors in the elastic constants propagate into the elastic moduli. The Young's modulus appears to be more affected by the choice of method than the bulk and shear moduli.

Table 5. The mean, standard deviation, and maximum of the absolute difference Δ in calculated results between the stress and approximate energy methods. The percentage of M_2AX phases with a difference below 10 and 20 GPa are also given. C_{13} shows the largest difference while C_{44} is the closest of the constants. The moduli B and G have the best agreement.

	Mean (GPa)	Std. dev. (GPa)	Max. (GPa)	$\Delta < 10$ GPa (%)	$\Delta < 20$ GPa (%)
C_{11}	4.4	5.6	46.0	90.8	97.7
C_{12}	3.5	5.2	51.3	94.5	98.6
C_{13}	12.8	5.4	33.6	30.4	90.8
C_{33}	5.5	6.7	57.3	86.2	96.3
C_{44}	1.8	2.4	28.4	99.1	99.5
B	5.3	2.2	15.7	97.7	100
G	2.9	2.4	18.0	98.6	100
E	5.6	5.8	43.3	86.6	97.2

3.2. Phases with extremal properties

One of the advantages of our comprehensive data set is that M_2AX phases with extremal properties can be identified. We are looking here for phases that stand out in any one of the parameters and are thus of potential interest for technological applications. In table 6, we present for several parameters (lattice parameters, elastic constants, elastic moduli, and the machinability indices) those phases with the largest and smallest values. Taking an overall look at the phases featured in this table, we see that several elements appear repeatedly. Phosphorus is the A element in all the phases with the largest elastic constants. As the softest A elements, cadmium, thallium and lead, dominate the phases with the smallest elastic constants. Cadmium is also the A element in all but one of the phases with the largest structural parameters. Of the M elements, tungsten, vanadium, tantalum, and chromium appear often in the table. Specific phases of interest are W_2CdN and W_2PN which have the largest and smallest c/a ratio of 5.5 and 3.2, respectively. These two phases could potentially give rise to interesting transport properties. Nb_2SC for instance, with a c/a of 3.5 (our calculation) is known to exhibit superconductivity [42]. Sc_2CdC and V_2PC have the largest and smallest interplanar separation between the M and A atomic layers (d_{MA}), respectively. As we will discuss below this parameter critically impacts the elastic properties of the M_2AX phases. Ta_2PN is the phase with the largest bulk modulus (255 GPa), while Sc_2CdC has the smallest with 73 GPa. This illustrates the wide range of bulk moduli through the M_2AX phase family.

For M_2AX phases to be used in a wide range of technological applications they must show good machinability, which is characterized here using two machinability indices: The Pugh [40] ductility index μ_D and the Sun *et al* [41] machinability index μ_M. The last two rows of table 6 identify the phases with the largest and smallest machinability indices. The phase with the largest ductility index of 8.1 is Ta_2PbN. The phase with the largest machinability index is W_2SnC ($\mu_M = 33.3$). Other phases with high machinability are Mo_2PbC ($\mu_M = 15.8$) and Cr_2PbN ($\mu_M = 12.2$). The machinability index is given by the ratio of bulk modulus to C_{44}. The motivation of this index being that useful materials have to be strong (i.e. high bulk modulus) as well as malleable (i.e. high shearability as indicated by a low C_{44}). The correlation between bulk modulus and C_{44} for our data set of M_2AX phases is shown in figure 2 with lines of constant machinability indicated. The slope of these lines increases with machinability. The data points adopt a broadly triangular distribution with all phases located above the unity machinability line. The phases with highest machinability (W_2SnC, Mo_2PbC and Cr_2PbN) are found near the vertical axis. This means that phases with high shearability (small C_{44}) tend to have a higher machinability than those with low shearability. The best example of this is W_2SnC which has the smallest C_{44} (6 GPa) of all the M_2AX phases.

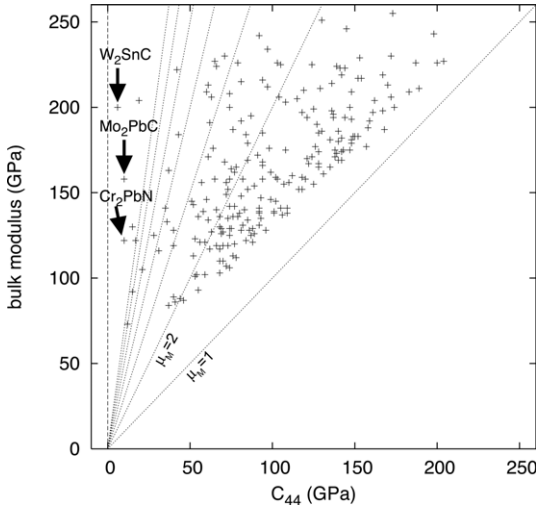

Figure 2. Correlation of M_2AX phase bulk moduli and C_{44} shear elastic constant ($\rho = 0.62$). Lines of constant machinability index $\mu_M = B/C_{44}$ are indicated. On this graph phases of highest machinability are located close to the vertical axis.

Table 6. M_2AX phases with extremal properties: the table lists the phases with the largest and smallest structural parameters (in Å), elastic constants, elastic moduli (in GPa), machinability index μ_M, and ductility index μ_D.

Property	Largest		Smallest	
	Phase	Quantity	Phase	Quantity
a	Zr_2AsC	3.484	Cr_2AlN	2.835
c	W_2CdN	15.83	Cr_2SC	10.47
d_{MX}	W_2CdN	1.436	Cr_2PbN	0.849
d_{MA}	Sc_2CdC	2.678	V_2PC	1.654
c/a	W_2CdN	5.520	W_2PN	3.208
C_{11}	Ta_2PC	384	Nb_2TlN	105
C_{12}	W_2PN	232	V_2CdC	0
C_{13}	W_2PC	239	Cr_2TlC	22
C_{33}	Ta_2PC	422	Sc_2CdC	130
C_{44}	V_2PC	204	W_2SnC	6
B	Ta_2PN	255	Sc_2CdC	73
G	V_2PC	154	Ta_2PbN	16
E	V_2PC	376	Ta_2PbN	46
μ_M	W_2SnC	33.33	V_2PC	1.11
μ_D	Ta_2PbN	8.13	Ti_2AlC	1.22

Table 7. List of property pairings with an absolute correlation coefficient $|\rho|$ larger than 0.7. Properties include lattice parameters, elastic constants, elastic moduli, atomic numbers, as well as row and column number of the M and A elements. G and E are analytically connected and thus have a very large coefficient.

		Correlation coefficient ρ		
Parameter 1	Parameter 2	M_2AX	M_2AC	M_2AN
G	E	+0.995	+0.995	+0.995
c	d_{MA}	+0.92	+0.96	+0.89
C_{13}	B	+0.92	+0.95	+0.90
C_{44}	E	+0.91	+0.92	+0.91
C_{33}	B	+0.91	+0.91	+0.90
C_{44}	G	+0.89	+0.90	+0.90
C_{11}	E	+0.84	+0.87	+0.80
C_{11}	G	+0.81	+0.84	+0.77
Column_A	d_{MA}	−0.80	−0.79	−0.81
C_{33}	d_{MA}	−0.79	−0.81	−0.76
C_{33}	C_{13}	+0.78	+0.79	+0.79
Row_A	d_{MA}	+0.76	+0.76	+0.77
Column_A	c	−0.76	−0.76	−0.75
C_{33}	C_{11}	+0.73	+0.78	+0.70
d_{MA}	B	−0.73	−0.74	−0.71
C_{33}	Row_A	−0.71	−0.67	−0.75
C_{12}	B	+0.71	+0.76	+0.71
C_{11}	B	+0.71	+0.72	+0.74
d_{MA}	z_A	+0.71	+0.70	+0.71
C_{33}	C_{44}	+0.70	+0.75	+0.66

3.3. Structure and elastic property correlations

Following on from the bulk modulus versus C_{44} correlation, we now survey our data set for other correlations between structural and elastic properties. Table 7 lists the correlation coefficients, ρ, between the lattice parameters, elastic constants C_{ij}, elastic moduli as well as the row, column, and atomic numbers of the M and A elements. The table lists all property pairs with a correlation coefficient of magnitude greater than or equal to 0.7. Several informative correlations become apparent in this data.

A large proportion of the correlations are found between the elastic moduli (B, G, and E) and the constants (C_{ij}). This is not surprising as the moduli are calculated from the constants. Also not surprising is the strong correlation between G and E elastic moduli ($\rho = 0.995$) considering that equation (3) simplifies to $E \sim 3G$ for $B \gg G$. This holds for most of the M_2AX phases which highlights the strong link between the shear and tensile behaviour in these materials.

More interesting is the strong correlation ($\rho = 0.92$) between the c lattice parameter and the interplanar separation d_{MA} in light of the fact that c and d_{MX} are poorly correlated ($\rho = 0.48$). This suggests that the unit cell dimensions in the c direction are determined much more by the A atomic layer than by the M_2X slab. We further find that d_{MA} is anti-correlated with the column number of the A element (column_A; $\rho = -0.80$) and correlated with the row number of the A element (row_A; $\rho = 0.76$). This is likely to be a reflection of the size of the A atom and the type of bonding between the M and A layers.

Looking now at correlations between structural parameters and elastic constants, the only correlation above the $|\rho| = 0.7$ threshold is between C_{33} and d_{MA} ($\rho = -0.79$).

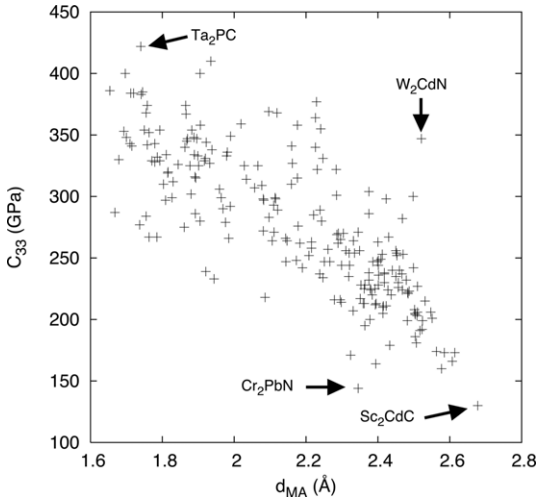

Figure 3. The correlation between the out-of-plane compressibility C_{33} and the MA interplanar separation d_{MA} ($\rho = -0.79$).

The data is shown in detail in figure 3. C_{33} describes the compressibility of the lattice in the c, or out-of-plane, direction in response to a strain in that direction. Therefore, the correlation suggests that longer MA bonds tend to make a M_2AX phase more compressible in the c direction. The importance of the A element to the elastic behaviour is also evident in the correlation ($\rho = -0.71$) between the row number of the A element (row_A) and C_{33}.

The importance of C_{33} to the overall elastic behaviour is evident in the fact that all but one of the other constants (namely, C_{12}) are correlated with C_{33} to $|\rho| > 0.7$. The elastic constants C_{13}, C_{11} and C_{44} have correlation coefficients with C_{33} of 0.78, 0.73, and 0.70, respectively. The correlations of C_{33} with C_{13} and C_{11} indicate that compressibility in the c direction (facilitated by the A element) translates into better compressibility in the in-plane direction. We hypothesize that a greater flexibility in the A atomic layer allows the M_2X slabs to deform into the c direction thus reducing in-plane stress. The correlation between C_{33} and C_{44} demonstrates the link between out-of-plane compressibility and shearability of the structure. The flexible nature of the MA bonds allows them to distort into both in- and out-of-plane directions, thereby affecting both compressibility and shearability of the M_2AX phases. Overall the elastic behaviour supports the idea that the A atomic layer acts as a flexible buffer between the more rigid M_2X slabs.

We now consider correlations between the carbide and nitride phases to elucidate the effect of the X element on the structural and elastic properties of M_2AX phases. Table 8 reports the correlation coefficients between M_2AC and M_2AN phases for structural parameters and elastic constants. Strong correlations indicate a minor effect created by the choice of X element whereas weak correlations indicate a greater role.

The universally high correlations between the structural parameters are straightforward to understand. The d_{MA} parameter ($\rho = 0.99$) is least sensitive to the choice of X element whilst d_{MX} ($\rho = 0.84$) is the most affected. For the elastic properties, the strongest correlation ($\rho = 0.93$) was found between the bulk moduli. Figure 4 shows

Table 8. Calculated correlation coefficients ρ between M_2AC and M_2AN phases, evaluated for lattice parameters and elastic constants.

a	c	d_{MX}	d_{MA}	C_{11}	C_{12}	C_{13}	C_{33}	C_{44}	B	G	E
0.89	0.94	0.84	0.99	0.59	0.63	0.84	0.91	0.85	0.93	0.71	0.73

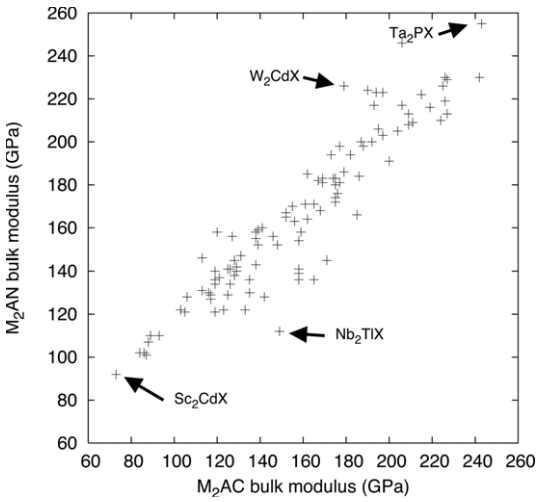

Figure 4. Correlation of calculated bulk moduli B between the M_2AN and M_2AC phases ($\rho = 0.93$).

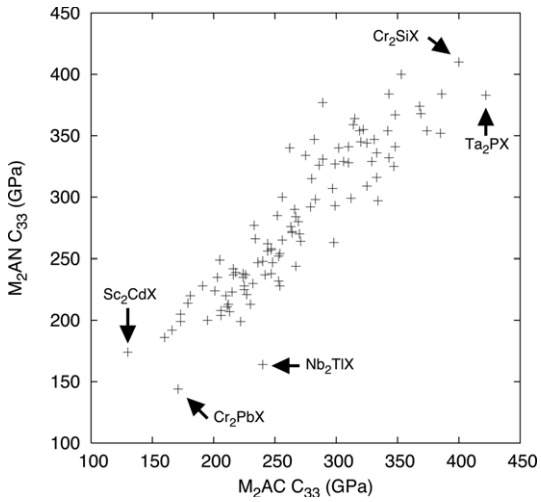

Figure 5. Correlation of the out-of-plane compressibility C_{33} between the M_2AN and M_2AC phases ($\rho = 0.91$).

the bulk modulus is almost unchanged between the M_2AC and M_2AN phases implying that the choice of X does not influence the compressibility of the material. This is consistent with our earlier observation that the MA bonds determine the compressibility in the c and in-plane directions. The correlation between C_{33} is almost as strong ($\rho = 0.91$; see figure 5) which further highlights the importance of the A layer (as opposed to the M_2X slab) to the out-of-plane compressibility. Similarly, the importance of the A layer to the shearing behaviour is evident in the high correlation found for C_{44} ($\rho = 0.85$) indicating a lesser role of the X element. The largest effect of the X element is found for the in-plane constants C_{11} and C_{12} which have the smallest correlation coefficients in the set ($\rho = 0.59$ and 0.63, respectively). For the C_{12} constant the data is shown in figure 6. This is further indicative [43] of the greater impact of the M_2X slab, and hence the X element, on the in-plane elastic properties. This contribution appears to result from the electronic structure of the MX bonds as opposed to the MX bond length, as both d_{MX} and a are highly correlated between the M_2AC and M_2AN phases.

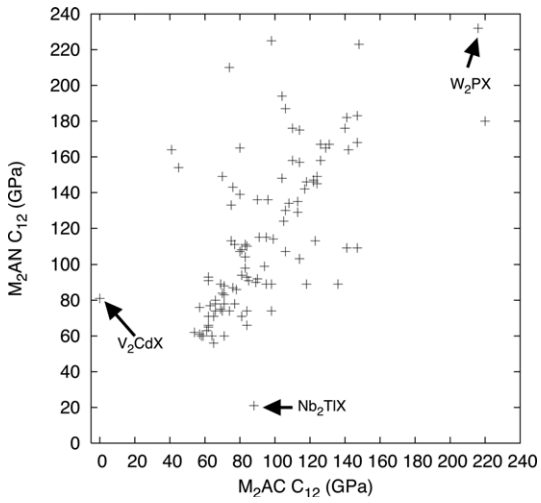

Figure 6. Correlation of C_{12} between the M_2AN and M_2AC phases ($\rho = 0.63$). The relatively weak correlation highlights the importance of the X element to the in-plane elastic behaviour of the M_2AX phases.

4. Summary and conclusions

The results and conclusions of this work can be summarized as follows:

(i) We have implemented and tested a method to calculate the elastic constants for 240 elemental compositions of the large M_2AX phase family of nanolaminate ceramics. Our discussion covered several of the specific technical issues that underpin such a large scale computational survey. These are: the choice of an accurate yet robust approach applicable to all 240 phases, our handling of numerical issues resulting in the loss of symmetry, as well as the effects of multiple stationary points on the potential energy surface.

(ii) Our survey has produced a large data base of structural parameters, elastic constants, and moduli for 240 M_2AX phases. This data base is included as supplementary data (available from stacks.iop.org/JPhysCM/21/305403) and it dramatically extends the existing knowledge about the elastic properties of this class of materials. Previous studies have been limited to isolated M_2AX phases [13–15, 17–19, 35–37] or smaller surveys on a limited

set of properties (e.g. the bulk modulus of 36 phases in [16] or C_{44} for 24 phases in [41]). The present work, in providing a full set of elastic constants for an effectively comprehensive set of elemental combinations, sets a new benchmark, allowing an assessment of M_2AX phase structure–property relations that cover the entire family.

(iii) We have presented and discussed detailed correlation analyses over the data. These reveal how various elastic and structural properties are related across the M_2AX phase family, and how they are influenced by the choice of elements. Specifically, the correlations reveal the governing role of the A element and its interaction with the M element in determining the c axis compressibility and shearability of the material. The role of the X element is relatively minor, with the strongest effect seen in the in-plane constants C_{11} and C_{12}. These findings offer strategies to tailor the elastic behaviour of the M_2AX phases by judicious choice of M, A, and X elements.

(iv) We have identified several elemental compositions that exhibit extremal properties. This serves to guide future research—experiment and theory—to elemental compositions with potentially unique materials properties. For instance, we identify the W_2SnC phase as having the lowest C_{44} constant indicating that it may be effective as a high-temperature dry lubricant.

References

[1] Barsoum M W and El-Raghy T 2001 *Am. Sci.* **89** 334
[2] Barsoum M W 2000 *Prog. Solid State Chem.* **28** 201
[3] Zhou Y C, Sun Z M, Sun J H, Zhang Y and Zhou J 2000 *Z. Metallk. d.* **91** 329
[4] Finkel P, Barsoum M W and El-Raghy T 2000 *J. Appl. Phys.* **87** 1701
[5] Sun Z M, Zhou Y C and Li M S 2001 *Corros. Sci.* **43** 1095
[6] Radhakrishnan R, Williams J J and Akinc M 1999 *J. Alloys Compounds* **285** 85
[7] Sun Z M, Hashimoto H, Zhang Z F, Yang S L and Tada S 2006 *Mater. Trans.* **47** 170
[8] El-Raghy T, Barsoum M W, Zavaliangos A and Kalidindi S R 1999 *J. Am. Ceram. Soc.* **82** 2855
[9] Zhou Y C and Sun Z M 1999 *Mater. Res. Innov.* **2** 360
[10] Barsoum M W, Yoo H I, Polushina I K, Rud V Y, Rud Y V and El-Raghy T 2000 *Phys. Rev.* B **62** 10194
[11] Barsoum M W, El-Raghy T, Rawn C J, Porter W D, Wang H, Payzant E A and Hubbard C R 1999 *J. Phys. Chem. Solids* **60** 429
[12] Istomin P V, Nadutkin A V, Ryabkov Y I and Goldin B A 2006 *Inorg. Mater.* **42** 250
[13] Holm B, Ahuja R, Li S and Johansson B 2002 *J. Appl. Phys.* **91** 9874
[14] Sun Z, Li S, Ahuja R and Schneider J M 2004 *Solid State Commun.* **129** 589
[15] Wang J Y and Zhou Y C 2004 *Phys. Rev.* B **69** 214111
[16] Sun Z, Music D, Ahuja R, Li S and Schneider J M 2004 *Phys. Rev.* B **70** 092102
[17] Bouhemadou A, Khenata R and Chegaar M 2007 *Eur. Phys. J.* B **56** 209
[18] Bouhemadou A and Khenata R 2007 *J. Appl. Phys.* **102** 043528
[19] Bouhemadou A, Khenata R, Kharoubi M and Medkour Y 2008 *Solid State Commun.* **146** 175
[20] Curtarolo S, Morgan D, Persson K, Rodgers J and Ceder G 2003 *Phys. Rev. Lett.* **91** 135503
[21] Morgan D, Rodgers J and Ceder G 2003 *J. Phys.: Condens. Matter* **15** 4361
[22] Blum V and Zunger A 2005 *Phys. Rev.* B **72** 069902
[23] Dudiy S V and Zunger A 2006 *Phys. Rev. Lett.* **97** 046401
[24] Greeley J and Mavrikakis M 2004 *Nat. Mater.* **3** 810
[25] Greeley J, Jaramillo T F, Bonde J, Chorkendorff I B and Nørskov J K 2006 *Nat. Mater.* **5** 909
[26] Greeley J and Norskov J K 2007 *Surf. Sci.* **601** 1590
[27] Ceder G, Chiang Y M, Sadoway D R, Aydinol M K, Jang Y I and Huang B 1998 *Nature* **392** 694
[28] Strasser P, Fan Q, Devenney M, Weinberg W H, Liu P and Nørskov J K 2003 *J. Phys. Chem.* B **107** 11013
[29] Kresse G and Hafner J 1993 *Phys. Rev.* B **47** 558
[30] Kresse G and Hafner J 1994 *Phys. Rev.* B **49** 14251
[31] Kresse G and Furthmüller J 1996 *Comput. Mater. Sci.* **6** 15
[32] Blöchl P E 1994 *Phys. Rev.* B **50** 17953
[33] Kresse G and Joubert D 1999 *Phys. Rev.* B **59** 1758
[34] Perdew J P, Chevary J A, Vosko S H, Jackson K A, Pederson M R, Singh D J and Fiolhais C 1992 *Phys. Rev.* B **46** 6671
[35] Hettinger J D, Lofland S E, Finkel P, Meehan T, Palma J, Harrell K, Gupta S, Ganguly A, El-Raghy T and Barsoum M W 2005 *Phys. Rev.* B **72** 115120
[36] Lofland S E, Hettinger J D, Harrell K, Finkel P, Gupta S, Barsoum M W and Hug G 2004 *Appl. Phys. Lett.* **84** 508
[37] Sun Z, Ahuja R, Li S and Schneider J M 2003 *Appl. Phys. Lett.* **83** 899
[38] Fast L, Wills J M, Johansson B and Eriksson O 1995 *Phys. Rev.* B **51** 17431
[39] Voigt W 1928 *Lehrbuch der Kristallphysik* (Leipzig: Taubner)
[40] Pugh S F 1954 *Phil. Mag.* **45** 823
[41] Sun Z, Music D, Ahuja R and Schneider J M 2005 *Phys. Rev.* B **71** 193402
[42] Sakamaki K, Wada H, Nozaki H, Onuki Y and Kawai M 1999 *Solid State Commun.* **112** 323
[43] Cover M F, Warschkow O, Bilek M M M and Mckenzie D R 2008 *Adv. Eng. Mater.* **10** 935